ACCEPTED MANUSCRIPT

# Pinning analyses of a BaHfO$_3$-containing GdBa$_2$Cu$_3$O$_{7-\delta}$ thin film grown by chemical solution deposition

# Pinning analyses of a BaHfO$_3$-containing GdBa$_2$Cu$_3$O$_{7-\delta}$ thin film grown by chemical solution deposition

Kazumasa Iida[1], Pablo Cayado[2], Hannes Rijckaert[3], Manuela Erbe[2], Jens Hänisch[2], Tatsunori Okada[4], Isabel Van Driessche[3], Satoshi Awaji[4], Bernhard Holzapfel[2]

[1]Department of Materials Physics, Nagoya University, Furo-cho, Chikusa-ku, Nagoya 464-8603, Japan

[2]Institute for Technical Physics, Karlsruhe Institute of Technology, Hermann-von-Helmholtz-Platz 1, 76344 Eggenstein-Leopoldshafen, Germany

[3]SCRiPTS, Department of Chemistry, Ghent University, Krijgslaan 281-S3, 9000 Ghent, Belgium

[4]High Field Laboratory for Superconducting Materials, Institute for Materials Research, Tohoku University, Katahira 2-1-1, Aoba-ku, Sendai 980-8577, Japan

E-mail: iida@mp.pse.nagoya-u.ac.jp, pablo.cayado@kit.edu

**Abstract.** The electric transport properties of a GdBa$_2$Cu$_3$O$_{7-\delta}$ thin film containing 12 mol% nano-sized BaHfO$_3$ (BHO) particles grown by chemical solution deposition were investigated in a wide range of temperatures ($4.2 \leq T \leq 77$ K) and magnetic fields up to $\mu_0 H = 19$ T. The exponent $n$ of the electric field–current density characteristics ($E \propto J^n$) has the following relation $(n-1) \propto J_c^\alpha$ ($\alpha \sim 0.45$) irrespective of measurement temperature for $H \parallel c$. On the other hand, this relation does not hold for $H \parallel ab$. The angular dependence of $J_c$ was almost similar to that of $n$ except for the angle close to the $ab$-plane. A dip of $n$ around this angle regime was observed below 77 K, whereas $J_c$ exhibited a maximum. At $T \leq 50$ K a tiny peak in the dip was observed that grew with decreasing temperatures. These results suggest that the pinning mechanism changes with temperature for $H \parallel ab$.

## 1. Introduction

$RE$Ba$_2$Cu$_3$O$_{7-\delta}$ ($RE$: rare earth elements, REBCO) compounds have been considered as technologically important superconductors thanks to their high critical temperature $T_c$ as well as high critical current performance even in the presence of high magnetic fields. Hence, tremendous efforts have been devoted to realise long length superconducting tapes, which led to the 2nd generation high-temperature-superconductor (HTS) technology, the coated conductors. However, the production costs of REBCO coated conductors are still high, which may delay practical applications.

2

Chemical solution deposition (CSD) based on metal-organic deposition (MOD) using trifluoroacetate (TFA) precursors has been considered as very cost-effective process for REBCO coated conductors [1, 2, 3]. Although many parameters have to be optimised for obtaining excellent superconducting performance, the superconducting properties of REBCO thin films grown by CSD are comparable to those of films fabricated by pulsed laser deposition (PLD) [4, 5].

To date, nano-sized perovskite-type particles have been incorporated in REBCO superconducting matrices to improve the critical current density $J_c$ in applied magnetic fields $H$ even further. In fact, nanoparticle addition improves the $J_c$–$H$ characteristics of REBCO grown by CSD dramatically without compromising $T_c$, which is in sharp contrast to PLD-grown REBCO films. For REBCO grown by PLD the modulation of nano-strain due to the self-assembled perovskite nano-rods triggers the depletion of oxygen, resulting in lower $T_c$ [6, 7]. To further improve the superconducting properties of CSD-grown REBCO, the underlying vortex pinning mechanism should be clarified.

Information on vortex pinning for a certain superconductor can be acquired by analysing i) the field dependence of $J_c$ and ii) the angular dependence of $J_c$ measured at various temperatures. Recently, the exponent $n$ in the power-law relation $E \propto J^n$ ($E$ electric field and $J$ current density) has gained much attention for analysing the pinning, since unlike for low–$T_c$ superconductors the exponent $n$ provides insight into both the sample's homogeneity [8] and vortex creep [9, 10]. The importance of analysing $n$ values for REBCO has been reported in several papers [11, 12, 13, 14, 15]. Here we report on the pinning mechanism of the CSD-grown GdBa$_2$Cu$_3$O$_{7-\delta}$+BaHfO$_3$ nanocomposite film by employing the methods mentioned above.

## 2. Experimental procedure

The GdBa$_2$Cu$_3$O$_{7-\delta}$ (GdBCO) thin film with 12 mol% nano-sized BaHfO$_3$ (BHO) particles was prepared by CSD. A concentration of 12 mol% of Ba$M$O$_3$ ($M$=Zr, Hf), corresponding to ~5 vol.%, has been considered optimum for CSD-grown REBCO (Ref. [14]), since tailoring of the Ba$M$O$_3$ nanoparticles in the superconducting matrix is difficult unless, e.g., employing the well-designed processing route proposed in Ref. [16]. The preparation of the TFA solution used in this work is reported in Ref. [17]. In summary, the Gd, Ba and Cu acetates (purity> 99.99%, Alfa Aesar) and the Hf(IV) 2,4-pentanedionate (97+%, Alfa Aesar) are weighed out to give a stoichiometric 1:2:3 ratio and a 12 mol% BHO concentration in the final films with regard to Gd. Subsequently, they are dissolved in water and trifluoroacetic acid (TFAH, 99.5+%, Alfa Aesar) to convert the acetates into trifluoroacetates. After removing the water and other impurities by a rotary evaporator, the final dry powder is re-diluted in absolute methanol (99.9%) adjusting the concentration to 0.25 mol/l in Gd. This solution is deposited on SrTiO$_3$(001) substrates via spin coating (6000 rpm for 30 s) and then the samples are pyrolyzed and grown using the optimized processes reported in [17] to finally obtain the GdBCO+12%BHO film studied in this work. As shown in [17], the GdBCO+12%BHO

films grow epitaxially with almost no traces of undesired secondary phases. Additionally, no preferred orientation of BHO is confirmed.

The microstructure of the films were investigated using high-resolution and scanning transmission electron microscopy (HRTEM and STEM) via a $C_s$-corrected JEOL JEM 2200-FS instrument operated at 200 kV with bright-field (BF) and high-angle annular dark field (HAADF) detectors. Cross-sectional TEM lamellae were prepared via the focused-ion-beam technique in a FEI Nova 600 Nanolab Dual-Beam microscopy. The lamellae were extracted using an *in–situ* lift-out procedure with an Omniprobe extraction needle.

After microstructural characterisation, a small bridge for transport measurements was structured by photolithographically and wet-chemical etching. The dimensions of the micro-bridge were 47 μm width, 1 mm length and 219 nm thickness, confirmed by atomic force microscopy (Bruker Dimension Edge AFM). To reduce the contact resistance, Au was deposited on the contact pads by PLD. The electrical resistivity was measured by a 4-probe method in a physical property measurement system (PPMS). The onset $T_c$ was determined as the intersection between the linear fit to the normal state resistivity and the steepest slope of resistivity. The irreversibility line was determined by the resistivity criterion $\rho_c = E_c/J_{c,10}$, where $E_c$ is the electrical field criterion of $1 \, \mu Vcm^{-1}$ for determining the critical current density $J_c$ and $J_{c,10}=10 \, Acm^{-2}$ is the corresponding criterion for the irreversibility field in $J_c$–$H$.

High-field electrical transport properties (d.c. fields up to $\mu_0 H=19 \, T$ with the 20 T cryogen-free superconducting magnet) were measured at IMR Tohoku university [18]. From $E$–$J$ characteristics, the critical current density $J_c$ was extracted using an electrical field criterion $E_c$ of $1 \, \mu Vcm^{-1}$. For measuring the angular dependence of $J_c$, the magnetic field $H$ was applied in maximum Lorentz force configuration at different angles $\theta$ measured from the $c$-axis. Only at 77 K the angular dependence of $J_c$ was measured in PPMS.

## 3. Results and discussion

BF-STEM image shows that the film is dense with only minimal porosity and the BHO nano-particles (NPs) are homogeneously distributed in the matrix (fig. 1(a)). It is also clear that a high density of intergrowths, called stacking faults (SFs) or $Gd_2Ba_4Cu_8O_{16}$ intergrowths and composed by double Cu-O planes, is observed in the upper region of the film. This tendency is quite common for CSD-grown REBCO films [19]. A more detailed view of the BHO NPs (fig. 1(b)) reveals that the average size of BHO is ∼20 nm. They tend to crystallise randomly oriented with respect to the surrounding GdBCO matrix. These NPs are surrounded by SFs (figs. 1(c) and (d)). It is also clear that BHO has faceted interfaces, which is similar to $BaZrO_3$ in YBCO grown by CSD [20]. Hence, highly incoherent interface between BHO and GdBCO is expected, which creates planar defects in CSD-grown films [21]. Those defects play an important role in the whole pinning scenario. The presence of the NPs generates a high-strain state distinguished by
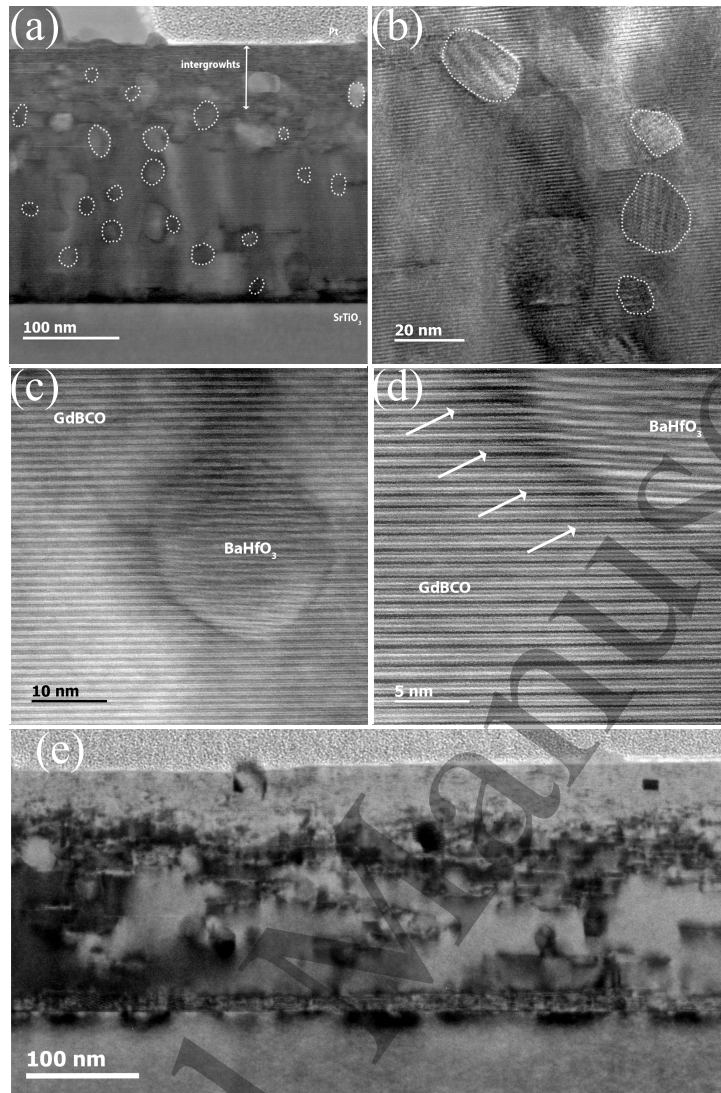
4



**Figure 1.** (a) Cross-sectional BF-STEM image of the GdBCO+12%BHO film grown on SrTiO$_3$. BHO nano-particles, which are surrounded by white dots for clarity, are finely dispersed in the superconducting matrix. High dense intergrowths is observed in the upper region of the film. (b) A more detailed view of the BHO NPs via HR-TEM reveals that the average size of BHO is ∼20 nm. They tend to crystallize randomly oriented with respect to the surrounding GdBCO matrix. (c) HAADF-STEM image of the interface between GdBCO and BHO. BHO has faceted interfaces, resulting in highly incoherent interface between BHO and GdBCO. (d) Several intergrowths presumably Gd$_2$Ba$_4$Cu$_8$O$_{16}$ indicated by white arrows are clearly seen in the high-resolution image of (c). (e) BF-TEM image taken with a diffraction vector $\vec{g} = (100)$. The black contrast indicates strain fields.

the black contrast in the cross-sectional BF-TEM image taken with a diffraction vector $\vec{g} = (100)$ (fig. 1(e)). Also, the SFs and NPs break the twin-boundaries, presumably reducing their pinning effectivity in the $c$-axis direction.

The onset $T_c$ was determined as 93.8 K (fig. 2(a)), which is comparable to our
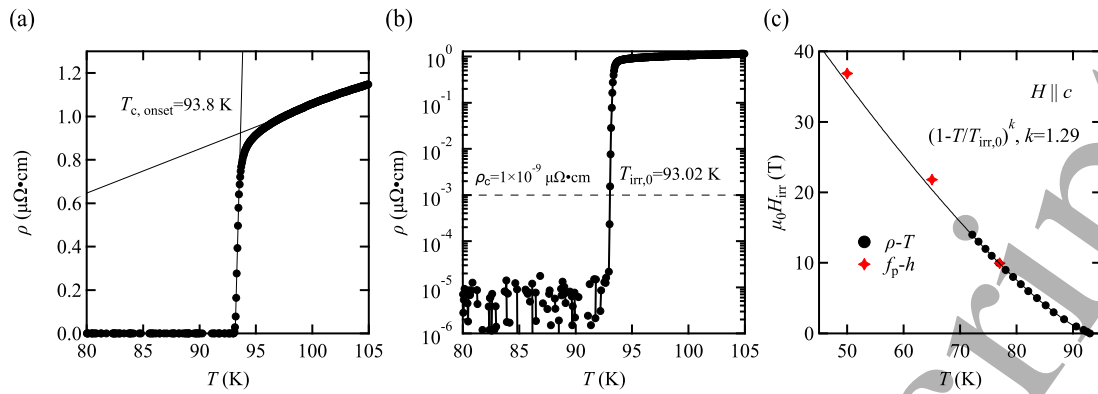
**Figure 2.** (a) Resistivity curve for GdBCO+BHO measured in the absence of magnetic field. (b) Semi-logarithmic plot of (a). Dashed line indicates the resistivity criterion for determining the irreversibility temperature $T_{\mathrm{irr}}$. In self-field the $T_{\mathrm{irr}}$ was 93.02 K. (c) The irreversibility line for $H \parallel c$ was determined by the field dependence of resistivity measurements. The irreversibility fields evaluated from the pinning force analyses well follows the irreversibility line.
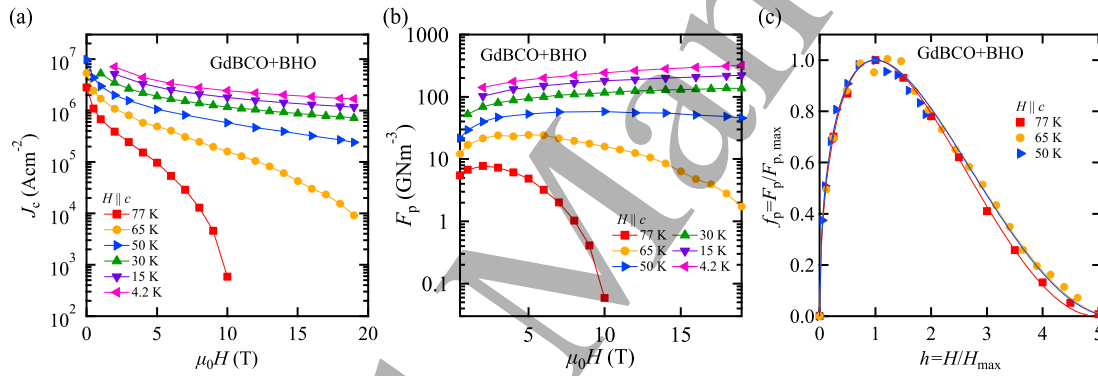


**Figure 3.** Field dependence of (a) $J_{\mathrm{c}}$ and (b) $F_{\mathrm{p}}$ for GdBCO+BHO measured at various temperatures. The applied field was parallel to the $c$-axis. Below 30 K and low field regime $J_{\mathrm{c}}$ could not be measured due to sample heating. (c) The normalised pinning force density $f_{\mathrm{p}} = F_{\mathrm{p}}/F_{\mathrm{p,max}}$ versus reduced field $h = H/H_{\mathrm{max}}$. Fits of eq. (1) to each $f_{\mathrm{p}}$ with fixed $q = 2$ is superimposed.

standard GdBCO grown by CSD [17]. The film showed a sharp transition of $\Delta T_{\mathrm{c}} = T_{\mathrm{c,onset}} - T_{\mathrm{irr,0}} \sim 0.8\,\mathrm{K}$, indicating a high quality of our film. The irreversibility line exhibits a power relation $\sim (1 - T/T_{\mathrm{irr,0}})^k$ with exponent $k$=1.29 (fig. 2(c)), which is close to the theoretically predicted value of 4/3 for glass-liquid transition in contrast to 3/2 for flux creep and 2 for melting [22].

Figure 3(a) summarises the $J_{\mathrm{c}}$–$H$ characteristics for GdBCO+BHO measured at various temperatures for $H \parallel c$. Self-field $J_{\mathrm{c}}$ and irreversibility field $H_{\mathrm{irr}}$ at 77 K were around 2.8 MAcm$^{-2}$ and $\sim$10 T, which is consistent with the result obtained from the resistivity measurements (fig. 2(c)). The maximum pinning force density $F_{\mathrm{p}}$ reached 7.8 GNm$^{-3}$ at 2 T at 77 K (fig. 3(b)). To acquire the information on vortex pinning

6

profoundly, the normalised pinning force $f_{\mathrm{p}} = F_{\mathrm{p}}/F_{\mathrm{p,max}}$ was plotted as a function of reduced field $h = H/H_{\mathrm{max}}$ (fig. 3(c)), where $F_{\mathrm{p,max}}$ is the maximum $F_{\mathrm{p}}$ and $H_{\mathrm{max}}$ is the field at which $F_{\mathrm{p}}$ shows the maximum value. If $f_{\mathrm{p}}$ is plotted as a function of $H/H_{\mathrm{max}}$ instead of $H/H_{\mathrm{irr}}$ as the usual practice for HTS, one can analyse the pinning mechanism even though $J_{\mathrm{c}}$ could not be measured up to $H_{\mathrm{irr}}$. Theoretically, $f_{\mathrm{p}}$ is described by the following formula,

$$f_{\mathrm{p}} = \left(\frac{p}{q}\right)^q h^p \left(\frac{p+q}{p} - h\right)^q, \tag{1}$$

which is analogous to the Dew-Hughes formula [23]. Substituting $(p, q)$=(0.5, 2) into eq. (1) leads to $f_{\mathrm{p}} = \frac{25}{16} h^{0.5} \left(1 - \frac{h}{5}\right)^2$, which is identical to $\left(\frac{H}{H_{\mathrm{irr}}}\right)^{0.5} \left(1 - \frac{H}{H_{\mathrm{irr}}}\right)^2$ [24]. As can be seen in fig. 3(c), eq. (1) fits well the data acquired at 77, 65 and 50 K with $p$=0.50, 0.46 and 0.47 under $q$=2. All values were close to 0.5, indicating that the flux movement is dominated by shear of the flux line lattice at low fields and by plastic deformation at high fields proposed by Kramer [25]. The data at 30, 15 and 4.2 K are excluded, since the $F_{\mathrm{p,max}}$ could not be reached in fields up to 19 T. It was reported that the interface between $BaZrO_3$ particles and the superconducting matrix in CSD-grown YBCO creates the strain fields. As the density of interfaces increases, a vast network of three-dimensional strained regions is constructed, resulting in quasi-isotropic pinning behaviour [20]. This mechanism may also prevail for GdBCO+BHO.

By using the exponent values $p$ and $q$, $H_{\mathrm{irr}}$ is calculated to be 10, 22 and 37 T at 77, 65 and 50 K, respectively. These values are well onto the irreversibility line shown in fig. 2(c).

Another direction for analysing the pinning mechanisms is to look at the $E$–$J$ characteristics for determining $J_{\mathrm{c}}$. For REBCO, the $E$–$J$ curves exhibit a power-law relation $E \propto J^n$ if the sample is homogeneous and free of grain boundaries. Since the exponent $n$ is proportional to the pinning potential, $J_{\mathrm{c}}$ usually scales positively with $n$ and empirically found a relation $(n-1) \propto J_{\mathrm{c}}^{\alpha}$ [27]. In fact, this can be seen in fig. 4(a). For $H \parallel c$ the relation $(n-1) \propto J_{\mathrm{c}}^{0.45}$ is almost followed irrespective of measurement temperature. The data for the high-$J_{\mathrm{c}}$ regime (i.e. below 65 K and low fields) deviate from the master curve towards lower $n$ values due probably to the second pinning mechanism setting in. Another plausible reason is that the scaling is valid for fields not too far away from $H_{\mathrm{irr}}$ only, since it is related to the critical exponents of the glass-liquid scaling. Somewhat higher $n$ values at 4 K compared to the scaling function might indicate slight Joule heating of the sample during measurement. For $H \parallel ab$ the data at 77 K falls onto the master curve $(n-1) \propto J_{\mathrm{c}}^{0.45}$ (fig. 4(b)), whilst all data at 65 and 50 K deviate from the master curve.

For further insight into the pinning mechanism, the angular dependence of $J_{\mathrm{c}}$ ($J_{\mathrm{c}}(\theta)$) and the corresponding $n(\theta)$ were measured at 77, 65, 50 and 30 K in various magnetic fields as summarised in fig. 5. Thanks to the BHO addition, the anisotropy of $J_{\mathrm{c}}$ (i.e. the ratio of $J_{\mathrm{c}}$ for $H \parallel ab$ and $c$) is rather small at low magnetic fields: e.g. $J_{\mathrm{c}}^{ab}/J_{\mathrm{c}}^{c}$ is around 1.4 at 77 and 65 K and 3 T. With increasing magnetic field towards $H_{\mathrm{irr}}$, a $J_{\mathrm{c}}$
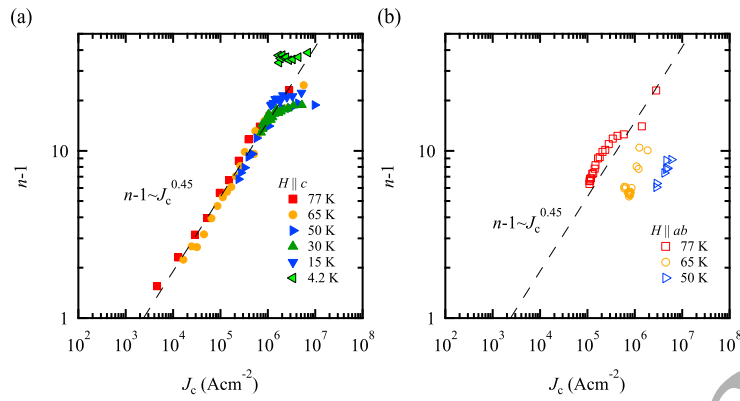
**Figure 4.** Relationship between $n$ and $J_c$ for (a) $H \parallel c$ and (b) $H \parallel ab$.

peak for $H \parallel c$ is progressively apparent, which is explained by the competition between random pinning and $c$-axis correlated growth defects, such as dislocations and anti-phase boundaries [33]. However, this peak is rather smeared at 50 K due to the small relative magnetic fields $H/H_{irr}$.

The angular dependence of $n$ behaves similarly to that of $J_c$ for the angle regime $-30° < \theta < 70°$. However, when the field direction is close to the $ab$-plane, the above scaling is violated. For $H \parallel ab$, the exponent $n$ shows a dip at 77 K in the low field regime, although $J_c$ shows a maximum (fig. 5(a)). But this dip disappears when the magnetic field is increased. Further increasing of $H$ leads to the upturn of $n$. Jha *et al.* recently showed very similar angular dependencies not for the $n$ value but rather for $J_c$ itself for PLD-grown $Y_2BaCuO_5$-YBCO nanocomposite films [28]. They explained this behaviour by a competition between different sets of pinning centres, namely the isotropic $Y_2BaCuO_5$ nanoparticles and the stacking faults, regarding their pinning potential, $U$. The same arguments may hold in our case: In the framework of Zeldov's model of a logarithmic current density dependence of the pinning potential [29], the $n$ value is directly related to $U$ [30]. The angular dependencies of $U$ are shown in [28]: Whereas isotropic defects show an angular dependence related (but not necessarily equal) to the electronic mass anisotropy, the correlated defects show a peak for fields parallel their direction, related to the accommodation of vortices in these defects for angles between the applied field and defect direction smaller than the so-called accommodation angle $\theta_{acc}$ ($\tan\theta_{acc} = \sqrt{2u_p/\epsilon_l}$, $u_p$ the pinning energy per unit length of the defect), which is related to line tension ($\epsilon_l$) of the vortices. This is exactly what is observed for high temperatures (77 K). At low fields, the pinning potential of the large random pinning centres ($BaZrO_3$ nanoparticles) surpass the pinning potential of the stacking faults leading to broad maxima of $n$ near $H \parallel c$ (with shoulders at intermediate angles). At high fields, the pinning potential of the correlated defects (both $ab$-directional stacking faults and $c$-directional growth defects such anti-phase boundaries and dislocations) is higher leading to peaks in $n$ value and $J_c$. The dip in $n$ value can be described and explained by scaling approaches taken into account the size
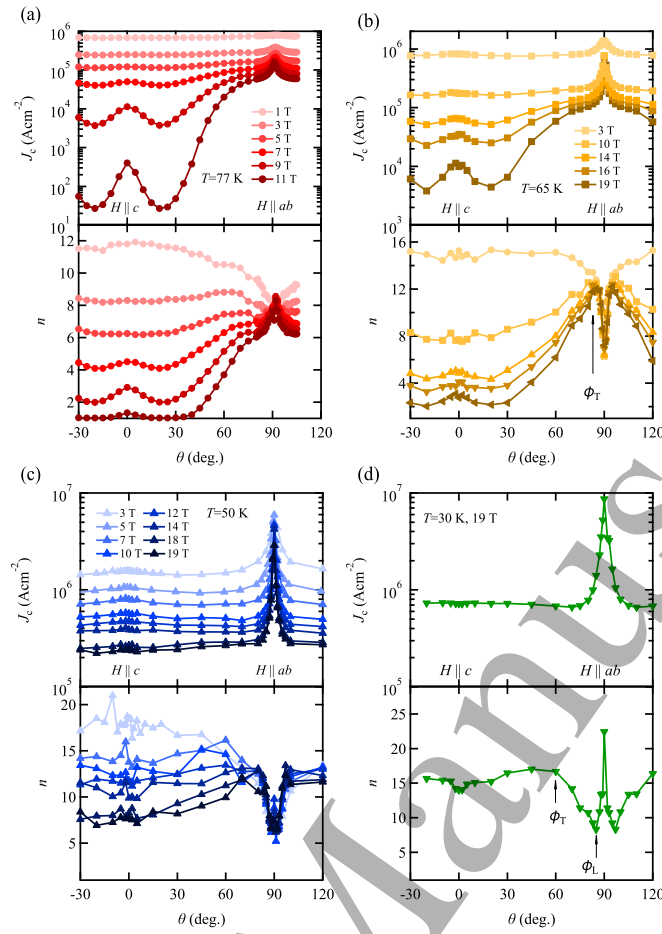
8



**Figure 5.** Angular dependence of $J_c$ and the corresponding $n$ value measured at (a) 77, (b) 65, (c) 50 and (d) 30 K in the presence of various magnetic fields.

of random pinning centres [31] or in statistical, maximum-entropy considerations [32]. The reason for the fact that these dependencies are observed for the $n$ value in our case but for $J_c$ in ref. [28] is not totally clear but may be related to the differences in microstructure, which is in reality much more complex.

At temperature of 65 K and below, the dip of $n$ near the $ab$-direction is formed at all magnetic fields investigated and the deep minimum is almost constant irrespective of applied magnetic fields. In contrast this minimum has a different reason. The dimensional crossover between the out-of-plane superconducting coherence length $\xi_c(T)$ and the $CuO_2$ interlayer distance $d$ occurs around this temperature, as also observed for TFA-MOD grown (Y,Gd)BCO films with $BaZrO_3$ [13] and pure YBCO grown by chemical vapour deposition [33]. The dip formation is due to the enhanced thermal movement of kinked vortices [34], since $n$ is fundamentally related to the flux creep rate $S = 1/(n-1)$ [35]. Parts of the vortices are trapped by the regions of reduced order parameter and connected by vortex kinks, thus forming a stair case structure. In contrast to the data at 77 K, $n(\theta)$ is independent of applied field within the dip (i.e. trapping) region since the creep rate, and hence the $n$ value, only depends on the number

of kinks per unit length of flux line.

The onset angle $\beta$ of the decrease of $n$ is related to the vortex trapping angle ($\phi_\mathrm{T}$), which is defined as $\phi_\mathrm{T}=90°-\beta$. The respective $\phi_\mathrm{T}$ at 65, 50 and 30 K at the maximum field are $5°$, $10°$ and $20°$. According to figs. 4(a), 5(a) and (b) the intrinsic pinning, originating from the modulation of the superconducting order parameter, starts to be active slightly above 65 K. The out-of-plane coherence length at zero kelvin, $\xi_c(0)$, is estimated to be $\sim 0.22$ nm by $\xi_c(0) = \frac{d}{2}\sqrt{1 - T_\mathrm{cr}/T_\mathrm{c}}$, where $d=\frac{2}{3}c=0.78$ nm ($c$ is the $c$-axis length determined by xrd) is the interlayer distance and $T_\mathrm{cr}$ is the the dimensional crossover temperature (i.e. $T_\mathrm{cr}\sim65$ K). The estimated value is close to the one for YBCO [36]. At 50 K, tiny peaks in the valley appear, and the peak grows prominently at 30 K. This phenomenon is related to the vortex lock-in, where all vortices are parallel to the $ab$-planes and locked between the CuO planes even though the applied field may incline slightly away from the planes. In this case, very strong pinning is created, the creep rate is decreased strongly due to the absence of kinks, and hence $n$ is increased. The respective vortex lock-in angle $\phi_\mathrm{L}$ at 50 and 30 K under $\mu_0 H=19$ T are around $2°$ and $5°$. It was reported that both $\phi_\mathrm{T}$ and $\phi_\mathrm{L}$ in YBCO are affected by nano-inclusions [37]. Both these characteristic angles for $BaZrO_3$-containing YBCO are larger than those for pure YBCO. It could be interesting to investigate if this tendency is also valid for GdBCO as assumed. These studies would be our future directions.

## 4. Conclusion

The pinning properties of a $GdBa_2Cu_3O_{7-\delta}$ thin film with 12 mol% of nano-sized $BaHfO_3$ (BHO) particles have been investigated by measuring field and angular dependence of electric transport $J_\mathrm{c}$ at various temperatures in fields up to 19 T. For $H \parallel ab$, $J_\mathrm{c}$ is dominated by intrinsic pinning below 77 K. The vortex trapping angle and lock-in angle are increased with decreasing temperature. The $n$-value analysis is a powerful tool for investigating the pinning mechanism especially for $H \parallel ab$.

## Acknowledgments

## References

[1] Knoth K, Engel S, Apetrii C, Falter M, Schlobach B, Hühne R, Oswald S, Schultz L and Holzapfel
     B, 2006 *Current Opinion in Solid State and Materials Science* **10** 205
[2] Albiss B A and Obaidat I M, 2010 *J. Mater. Chem.* **20** 1836
[3] Bäcker M, Baumann A, Brunkahl O, Erbe M and Schneller T, 2020 Chemical Solution Deposition
     (CSD) *Encyclopedia of Applied Physics*, Wiley   VCH Verlag GmbH and Co. KGaA (Ed.).

10

[4] Erbe M, Hänisch J, Hühne R, Freudenberg T, Kirchner A, Molina-Luna L, Damm C, Van Tendeloo G, Kaskel S, Schultz L and Holzapfel B, 2015 *Supercond. Sci. Technol.* **28** 114002

[5] Rijckaert H, Cayado P, Nast R, Sierra J, Erbe M, Dominguez P, Hänisch J, De Buysser K, Holzapfel B and Van Driessche I, 2020 *Coatings* **10** 17

[6] Cantoni C, Gao Y, Wee S H, Specht E D, Gazquez J, Meng J, Pennycook S J and Goyal A, 2011 *ACS Nano* **5** 4783

[7] Horide T, Kametani F, Yoshioka S, Kitamura T and Matsumoto K, 2017 *ACS Nano* **11** 1780

[8] Warnes W. H and Larbalestier D. C, 1986 *Appl. Phys. Lett.* **48** 1403

[9] Yeshurun Y, Malozemoff A P and Shaulov A 1996 *Rev. Mod. Phys* **68** 911

[10] Sun J Z, Eom C B, Lairson B, Bravman J C and Geballe T H, 1991 *Phys. Rev. B* **43** 3002

[11] Civale L, Maiorov B, MacManus-Driscoll J L, Wang H, Holesinger T G, Foltyn S R, Serquis A and Arendt P N, 2005 *IEEE. Trans. Appl. Supercond.* **15** 2808

[12] Tarantsev E F, Strickland N M, Hoefakker P, Xia J A and Long N J, 2008 *Current Applied Physics* **8** 388

[13] Awaji S, Namba M, Watanabe K, Miura M, Yoshizumi M, Izumi T and Shiohara Y, 2010 *Supercond. Sci. Technol.* **23** 014006

[14] Palau A, Bartolomé E, Llordés A, Puig T and Obradors X, 2011 *Supercond. Sci. Technol.* **24** 125010

[15] Chudy M, Zhong Z, Eisterer M and Coombs T, 2015 *Supercond. Sci. Technol.* **28** 035008

[16] Miura M, Maiorov B, Sato M, Kanai M, Kato T, Kato T, Izumi T, Awaji S, Mele P, Kiuchi M and Matsushita T, 2017 *NPG Asia Mater.* **9** e447

[17] Cayado P, Erbe M, Kauffmann-Weiss S, Bühler C, Jung A, Hänisch J and Holzapfel B, 2017 *Supercond. Sci. Technol.* **30** 094007

[18] Awaji S, Oguro H, Watanabe K, Hanai S, Ioka S, Miyazaki H, Daibo M, Iijima Y, Saito T and Itoh M, 2014 *Adv. Cryo. Eng.* **59** 732

[19] Li Z, Coll M, Mundet B, Chamorro N, Vallés F, Palau A, Gazquez J, Ricart S, Puig T and Obardors X 2019 *Sci. Rep.* **9** 5828

[20] Llordés A, Palau A, Gázquez J, Coll M, Vlad R, Pomar A, Arbiol J, Guzmán R, Ye S, Rouco V, Sandiumenge F, Ricart S, Varela M, Chateigner D, Vanacken J, Gutiérrez J, Moshchalkov V, Deutscher G, Magen C and Obradors X, 2012 *Nat. Mater.* **6** 367-73

[21] Molina-Luna L, Duerrschnabel M, Turner S, Erbe M, Martinnez G T, Van Aert S, Holzapfel B and Van Tendeloo G, 2015 *Supercond. Sci. Technol.* **28** 115009

[22] Schilling A, Ott H R and Wolf Th, 1992 *Phys. Rev. B* **46** 14253

[23] Dew-Hughes D, 1974 *Philos. Mag.* **30** 293

[24] Higuchi T, Yoo S I and Murakami M, 1999 *Phys. Rev. B* **59** 1514

[25] Kramer E J, 1973 *J. Appl. Phys.* **44** 1360

[26] Awaji S, Namba M, Watanabe K, Ito S, Aoyagi E, Kai H, Mukaida M and Okayasu S, 2011 *IEEE. Trans. Appl. Supercond.* **21** 3192

[27] Opherden L, Sieger M, Pahlke P, Hühne R, Schultz L, Meledin A, Van Tendeloo G, Nast R, Holzapfel B, Bianchetti M, MacManus J L and Hänisch J, 2016 *Sci. Rep.* **6** 21188

[28] Jha A K, Matsumoto K, Horide T, Saini S, Mele P, Ichinose A, Yoshida Y and Awaji S, 2017 *J. Appl. Phys.* **122** 093905

[29] Zeldov E, Amer N M, Koren G, Gupta A, McElfresh M W and Gambino R J, 1990 *Appl. Phys. Lett.* **56** 680

[30] Guarino A, Leo A, Grimaldi G, Martucciello N, Dean C, Kunchur M N, Pace S and Nigro A 2014 *Supercond. Sci. Technol.* **27** 124011

[31] Mishev V, Zehetmayer M, Fischer D X, Nakajima M, Eisaki H and Eisterer M 2015 *Supercond. Sci. Technol.* **28** 102001

[32] Long N J, 2013 *J. Supercond. Nov. Magn.* **26** 763

[33] Awaji S, Ishihara R, Watanabe K, Shikimachi K, Hirano N and Nagaya S, 2011 *Appl. Phys. Express* **4** 013101

11

[34] Maiorov B, Baily S. B, Zhou H, Ugurlu O, Kennison J. A, Dowden P. C, Holesinger T. G, Foltyn S. R and Civale L, 2009 *Nat. Mater.* **8** 398

[35] Yamasaki H and Mawatari Y, 1999 *IEEE. Trans. Appl. Supercond.* **9** 2651

[36] Camerlingo C and Jung G, 2005 *Supercond. Sci. Technol.* **18** 1106

[37] Weigand M, Zhou H, Foltyn S R, Civale L and Maiorov B, 2012 Temperature dependence of pinning near $H \parallel ab$ in YBCO thin films *Applied Superconductivity conference* 3ME-03